A quasistatic contact model for impact analysis in flexible multibody systems based on IGA

Tobias Rückwald, Alexander Held, Robert Seifried

Institute of Mechanics and Ocean Engineering
Hamburg University of Technology
Eißendorfer Straße 42, 21073 Hamburg, Germany
[tobias.rueckwald,alexander.held,robert.seifried]@tuhh.de

ABSTRACT

A rather new approach for detailed impact simulations in flexible multibody systems is based on reduced isogeometric analysis (IGA) models. A precise impact simulation requires an accurate representation of the deformation in the contact area, which can be obtained using the Craig-Bampton method for model reduction. However, the resulting equations of motion are numerically stiff and therefore computationally expensive to solve. In literature, a quasistatic contact model for isoparametric elements has been proposed to reduce the numerical stiffness. It neglects the dynamics of the local deformations in the contact area. This work applies this quasistatic contact model to the IGA model within the floating frame of reference approach. In the application example, the impact of two flexible double pendulums is simulated. This setup includes large rigid body motions and small elastic deformations.

Keywords: IGA, impact, contact, flexible multibody system, quasistatic.

1 INTRODUCTION

Impacts within flexible multibody systems often include large rigid body motions before and after impact. Elastic deformations remain small if stiff materials, e.g. steel or aluminum, are selected. These conditions favor the floating frame of reference formulation [1] in the modeling of the flexible bodies. The use of the floating frame of reference formulation requires global shape functions $\mathbf{\Phi}$ to describe body flexibility. The global shape functions can be obtained with finite element methods, e.g. isoparametric elements. A disadvantage of isoparametric elements is that the geometry is discretized. However, detailed impact simulations depend on an accurate representation of the geometry in the contact area. As an alternative approach, the isogeometric analysis (IGA) [2] can be used to model the flexible body, since there is no error in the representation of the geometry. In the context of efficient and accurate flexible multibody impact simulations, the global shape functions are retrieved by model reduction. A straightforward reduction approach is modal reduction. However, modal reduction does not consider the precise local deformation in the contact area. This leads to inaccurate results, as shown in [3]. Alternatively, the Craig-Bampton method [4] can be used. It approximates the overall elastodynamic behavior by "low" frequency normal modes and local deformations in the contact area by constrained modes introducing numerically very high frequencies. However, the combination of "low" and "high" frequency modes leads to numerically stiff system equations requiring small time step sizes in the numerical integration. As an example, in a rigid body motion before impact, the "high" frequency modes are not yet excited allowing larger step sizes. An occurring impact results in local deformations exciting the "high" frequency modes. The current and subsequent impacts require small step sizes, including the intervening rigid body motions. It is shown in [5] that the "high" frequency modes only have small influence on the dynamics. A quasistatic contact model based on isoparametric elements is introduced in [5], which neglects the dynamics of the "high" frequency modes. Thereby, the numerical stiffness is reduced and the numerical efficiency is increased. The aim of this work is to adapt the idea of a quasistatic contact model to the IGA. The computational performance is to be improved during impacts and

subsequent rigid body motions.
This work is organized in the following way: The floating frame of reference formulation is briefly summarized in Section 2. Section 3 introduces the concepts of the IGA and the determination of the global shape functions. The contact algorithm, the quasistatic contact model as well as the overall simulation procedure are detailed in Section 4. The following Section 5 provides a detailed discussion of an application example, and the results are summarized in Section 6.

2 FLOATING FRAME OF REFERENCE FORMULATION

The floating frame of reference formulation is a well-established approach when modeling flexible multibody systems [1]. Large nonlinear rigid body motion of the body reference frame $\mathrm{K_R}$ are described within the inertial frame $\mathrm{K_I}$. This work utilizes Buckens- and tangent-frames [1] as floating frames. Given that the body deformations remain small and linear elastic, they can be described conveniently in the body frame $\mathrm{K_R}$. Then, elastic deformations can be approximated by n_q global shape functions $\boldsymbol{\Phi} = \begin{bmatrix}\boldsymbol{\Phi}_1 & \dots & \boldsymbol{\Phi}_{\mathrm{n_q}}\end{bmatrix}$ and their corresponding elastic coordinates $\mathbf{q}_\mathrm{e}$. The equations of motion for a free flexible body are given by

$$\underbrace{\begin{bmatrix} m\mathbf{E} & m\tilde{\mathbf{c}}^\mathsf{T} & \mathbf{C}_\mathrm{t}^\mathsf{T} \\ m\tilde{\mathbf{c}} & \mathbf{I} & \mathbf{C}_\mathrm{r}^\mathsf{T} \\ \mathbf{C}_\mathrm{t} & \mathbf{C}_\mathrm{r} & \overline{\mathbf{M}}_\mathrm{e} \end{bmatrix}}_{\mathbf{M}} \underbrace{\begin{bmatrix} {}^\mathrm{R}\dot{\mathbf{v}}_\mathrm{IR} \\ {}^\mathrm{R}\dot{\boldsymbol{\omega}}_\mathrm{IR} \\ \ddot{\mathbf{q}}_\mathrm{e} \end{bmatrix}}_{\dot{\mathbf{z}}_\mathrm{II}} = \underbrace{\begin{bmatrix} \mathbf{h}_\mathrm{dt} \\ \mathbf{h}_\mathrm{dr} \\ \mathbf{h}_\mathrm{de} \end{bmatrix}}_{\mathbf{h}_\mathrm{d}} + \underbrace{\begin{bmatrix} \mathbf{h}_\mathrm{bt} \\ \mathbf{h}_\mathrm{br} \\ \mathbf{h}_\mathrm{be} \end{bmatrix}}_{\mathbf{h}_\mathrm{b}} - \underbrace{\begin{bmatrix} \mathbf{h}_{\omega\mathrm{t}} \\ \mathbf{h}_{\omega\mathrm{r}} \\ \mathbf{h}_{\omega\mathrm{e}} \end{bmatrix}}_{\mathbf{h}_\omega} - \underbrace{\begin{bmatrix} \mathbf{0} \\ \mathbf{0} \\ \overline{\mathbf{K}}_\mathrm{e}\mathbf{q}_\mathrm{e} + \overline{\mathbf{D}}_\mathrm{e}\dot{\mathbf{q}}_\mathrm{e} \end{bmatrix}}_{\mathbf{h}_\mathrm{e}}, \tag{1}$$

where $\mathbf{E}$ is the identity matrix, ${}^\mathrm{R}\mathbf{v}_\mathrm{IR}$ is the absolute velocity of the reference frame, and ${}^\mathrm{R}\boldsymbol{\omega}_\mathrm{IR}$ is the angular velocity. In Eq. (1), the mass of the body is denoted by m, the center of mass relative to $\mathrm{K_R}$ by $\mathbf{c}$, the translational and rotational coupling matrices by $\mathbf{C}_\mathrm{t}$ and $\mathbf{C}_\mathrm{r}$, the mass moment of inertia by $\mathbf{I}$, and the mass, stiffness, and damping matrix of the flexible body by $\overline{\mathbf{M}}_\mathrm{e}$, $\overline{\mathbf{K}}_\mathrm{e}$, and $\overline{\mathbf{D}}_\mathrm{e}$. The right-hand side of Eq. (1) is composed of the vector of discrete forces $\mathbf{h}_\mathrm{d}$, such as contact forces, the body forces $\mathbf{h}_\mathrm{b}$, the generalized inertial forces $\mathbf{h}_\omega$, and the internal forces $\mathbf{h}_\mathrm{e}$. The required data to evaluate the equations of motion of a free flexible body are provided by the standard input data (SID) [1].

3 GLOBAL SHAPE FUNCTIONS FROM IGA

Determining the global shape functions $\boldsymbol{\Phi}$ is a key issue in using the floating frame of reference formulation. The straightforward approach is to generate a finite element model of the flexible body and apply a model reduction technique. This section briefly presents the idea of the IGA and the Craig-Bampton method to obtain the global shape functions $\boldsymbol{\Phi}$ via model reduction. A more detailed introduction to the IGA can be found in [2]. It is worth mentioning that hierarchical refinement is used as local refinement in this work. Interested readers are referred to [6] for more details.

3.1 Basis splines

The IGA consists of three spaces: the physical space, the parameter space, and the index space. For simplicity, only the first two spaces will be discussed in the following. The parameter space and the physical space are visualized in Fig. 1. The parameter space consists of the local coordinates ξ, η, and ζ. The knot vectors $\boldsymbol{\Xi} = \begin{bmatrix}\xi_1 & \xi_2 & \dots & \xi_{\mathrm{n+p+1}}\end{bmatrix}$, $\boldsymbol{\mathcal{H}} = \begin{bmatrix}\eta_1 & \eta_2 & \dots & \eta_{\mathrm{m+q+1}}\end{bmatrix}$, and $\boldsymbol{\mathcal{Z}} = \begin{bmatrix}\zeta_1 & \zeta_2 & \dots & \zeta_{\mathrm{m+q+1}}\end{bmatrix}$ span up the parameter space and its elements. Additionally, the n, m, and ℓ local shape functions $N_{i,\mathrm{p}}$, $M_{j,\mathrm{q}}$, and $L_{k,\mathrm{r}}$ of order p, q, and r are defined in the parameter space in the respective local coordinate direction. The local shape functions are based on B-splines, which

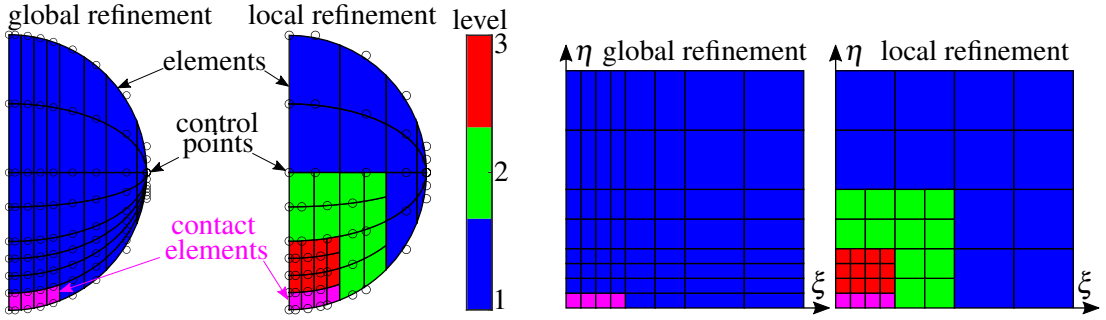

(a) Physical space. (b) Parameter space.

Figure 1: Example of an axisymmetric sphere that should be refined in the contact area.

can be computed recursively with the Cox-de Boor algorithm,

$$p=0: \quad N_{i,0}(\xi)=\begin{cases} 1 & \text{if } \xi_i \le \xi < \xi_{i+1} \\ 0 & \text{otherwise} \end{cases} \tag{2}$$

$$p>1: \quad N_{i,\mathrm{p}}(\xi)=\frac{\xi-\xi_i}{\xi_{i+\mathrm{p}}-\xi_i}N_{i,\mathrm{p}-1}(\xi)+\frac{\xi_{i+\mathrm{p}+1}-\xi}{\xi_{i+\mathrm{p}+1}-\xi_{i+1}}N_{i+1,\mathrm{p}-1}(\xi). \tag{3}$$

The same formalism in Eq. (2) and Eq. (3) holds for $M_{j,\mathrm{q}}$ and $L_{k,\mathrm{r}}$ in η- and ζ-direction. Since recursive functions are numerically inefficient, a non-recursive algorithm suggested in [7] is used.

3.2 Non-uniform rational basis splines

As visualized in Fig. 1, the physical space consists of the control points $\mathbf{P}_{i,j,k}$, which are arranged by the control net. The task of the control points is to span the geometry in the physical space. The number of control points is identical to the number of basis functions resulting in a net of $n \times m \times \ell$ control points. In addition to the physical position, each control point has a weight $w_{i,j,k}$. The transformation from the parameter space into the physical space requires the non-uniform rational basis splines (NURBS) basis $R^{\mathrm{p,q,r}}_{i,j,k}(\xi,\eta,\zeta)$ given by

$$R^{\mathrm{p,q,r}}_{i,j,k}(\xi,\eta,\zeta)=\frac{N_{i,\mathrm{p}}(\xi)M_{j,\mathrm{q}}(\eta)L_{k,\mathrm{r}}(\zeta)w_{i,j,k}}{\sum_{\hat{i}=1}^{\mathrm{n}}\sum_{\hat{j}=1}^{\mathrm{m}}\sum_{\hat{k}=1}^{\ell}N_{\hat{i},\mathrm{p}}(\xi)M_{\hat{j},\mathrm{q}}(\eta)L_{\hat{k},\mathrm{r}}(\zeta)w_{\hat{i},\hat{j},\hat{k}}}. \tag{4}$$

The NURBS basis $R^{\mathrm{p,q,r}}_{i,j,k}(\xi,\eta,\zeta)$ and the control points $\mathbf{P}_{i,j,k}$ then lead to a NURBS solid

$$\mathbf{S}=\sum_{i=1}^{\mathrm{n}}\sum_{j=1}^{\mathrm{m}}\sum_{k=1}^{\ell}R^{\mathrm{p,q,r}}_{i,j,k}(\xi,\eta,\zeta)\mathbf{P}_{i,j,k} \tag{5}$$

in the physical space. The deformation $\mathbf{d}$ can be written in matrix-vector notation as

$$\mathbf{d}=\mathbf{N}\mathbf{u}=\begin{bmatrix} R^{\mathrm{p,q}}_{1,1,1} & 0 & 0 & \dots & 0 \\ 0 & R^{\mathrm{p,q}}_{1,1,1} & 0 & \dots & 0 \\ 0 & 0 & R^{\mathrm{p,q,r}}_{1,1,1} & \dots & R^{\mathrm{p,q,r}}_{\mathrm{p+1,q+1,r+1}} \end{bmatrix} \begin{bmatrix} u^{\mathrm{x}}_{1,1,1} \\ u^{\mathrm{y}}_{1,1,1} \\ u^{\mathrm{z}}_{1,1,1} \\ \vdots \\ u^{\mathrm{z}}_{\mathrm{p+1,q+1,r+1}} \end{bmatrix}, \tag{6}$$

where the basis functions of the corresponding element are summarized in the matrix $\mathbf{N}$ and the displacements of the control points in $\mathbf{u}$.

3.3 Model order reduction

As with the floating frame of reference formulation, it is assumed that only small elastic deformations occur. Therefore, linear elasticity is assumed and the weak Galerkin method is applied as for

isoparametric elements [8]. From this, the equations of motion of the assembled IGA based finite element model are given by

$$\mathbf{M}_\mathrm{e}\ddot{\mathbf{u}}_\mathrm{e} + \mathbf{K}_\mathrm{e}\mathbf{u}_\mathrm{e} = \mathbf{0}, \tag{7}$$

where $\mathbf{M}_\mathrm{e}$ is the full mass matrix, $\mathbf{K}_\mathrm{e}$ the full stiffness matrix, and $\mathbf{u}_\mathrm{e}$ the displacements of the control points. For the incorporation of the isogeometric model into the equations of motion (1), the global shape functions $\mathbf{\Phi}$ are required. A simple and straightforward approach for reducing the full finite element model (7) is modal truncation. However, the "low" frequency eigenmodes typically are not able to precisely describe local deformation in the contact area. This leads to inaccurate results, as shown in [3]. Alternatively, the Craig-Bampton method [4] is used. The Craig-Bampton method combines fixed-interface normal modes and constraint modes. The normal modes represent the overall flexibility and the constraint modes modes approximate the deformation in a specific area, e.g. the contact area. The constraint modes require the selection of predefined control points on the exterior surface. The procedure results in the global shape functions $\mathbf{\Phi}$, which are orthogonalized and normalized to the mass matrix. The reduced mass and stiffness matrix are then given by

$$\overline{\mathbf{M}}_\mathrm{e} = \mathbf{\Phi}^\mathsf{T}\mathbf{M}_\mathrm{e}\mathbf{\Phi} = \mathbf{E} \qquad \text{and} \qquad \overline{\mathbf{K}}_\mathrm{e} = \mathbf{\Phi}^\mathsf{T}\mathbf{K}_\mathrm{e}\mathbf{\Phi} = \mathrm{diag}(\omega_i^2), \tag{8}$$

respectively, where ω_i are the eigenfrequencies. A key issue of the Craig-Bampton method is the numerical stiffness of the equations of motion (1). This is due to "low" frequency normal modes and the "high" frequency constrained modes. A simple method to improve the numerical performance is to modally damp the "high" frequency modes. This method has been already applied in IGA impact simulations [6].

4 CONTACT HANDLING IN IGA

Besides modal damping, a quasistatic contact model can be used to improve numerical performance of the contact simulation. This section details a contact algorithm of IGA bodies in flexible multibody systems, introduces the concept of a quasistatic contact model and proposes a contact simulation procedure.

4.1 Contact evaluation

Several methods exist for discretizing the contact of two IGA bodies. This work uses a Node-to-segment method. This is more efficient than an integral description, but the accuracy is still comparable [9]. In the course of a node-to-segment method, a predefined contact interval is discretized using a collocation method, e.g. Botella points [9]. This collocation method is paired with a penalty method for contact treatment. The corresponding penalty factor c_p is generally chosen heuristically. Thereby, the penalty factor should be chosen large enough such that the results become independent of the chosen parameter [10]. Increasing the penalty factor beyond its converging value also increases the numerical stiffness of the equations of motion (1). This results in a higher computation time or the numerical integration might even terminate unsuccessfully.
The contact is evaluated in the inertial frame $\mathrm{K_I}$. Therefore, the positions of the deformed control points ${}^\mathrm{I}\mathbf{P}_{i,j,k}$ in the inertial frame are required. The positions of the deformed control points are composed of the undeformed control points ${}^\mathrm{R}\mathbf{P}^0_{i,j,k}$ and the elastic deformation $\mathbf{u}_{\mathrm{e},i,j,k}$ based on the global shape functions $\mathbf{\Phi}_{i,j,k}$ and the elastic coordinates $\mathbf{q}_\mathrm{e}$ as

$${}^\mathrm{R}\mathbf{P}_{i,j,k} = {}^\mathrm{R}\mathbf{P}^0_{i,j,k} + \mathbf{u}_{\mathrm{e},i,j,k} = {}^\mathrm{R}\mathbf{P}^0_{i,j,k} + \mathbf{\Phi}_{i,j,k}\mathbf{q}_\mathrm{e}. \tag{9}$$

The absolute positions of the control points are given by

$${}^\mathrm{I}\mathbf{P}_{i,j,k} = \mathbf{S}_\mathrm{IR}(\boldsymbol{\beta}_\mathrm{IR})\left({}^\mathrm{R}\mathbf{r}_\mathrm{IR} + {}^\mathrm{R}\mathbf{P}_{i,j,k}\right) \tag{10}$$

requiring the reference frame position ${}^\mathrm{R}\mathbf{r}_\mathrm{IR}$ and the rotational parameters $\boldsymbol{\beta}_\mathrm{IR} \in \varepsilon^3$. The rotation matrix $\mathbf{S}_\mathrm{IR}(\boldsymbol{\beta}_\mathrm{IR})$ is determined with Cardan angles. In the course of contact evaluation, one body is

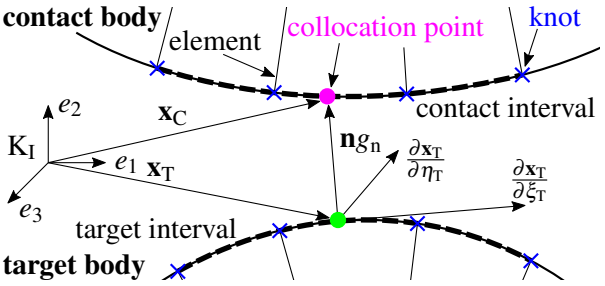

Figure 2: Contact detection between the contact and target body.

defined as contact body and the other as target body, as depicted in Fig. 2. The collocation points are located on the exterior surface of the contact body within the contact area and are tested for contact with the exterior surface of the target body. As an example, a surface with the local coordinates ξ_T and η_T is integrated, keeping ζ_T constant. The contact of two bodies is checked by solving the nonlinear equation

$$\left[\frac{\partial \mathbf{x}_T(\xi_T,\eta_T,\zeta_T)}{\partial \xi_T} \quad \frac{\partial \mathbf{x}_T(\xi_T,\eta_T,\zeta_T)}{\partial \eta_T}\right]^T (\mathbf{x}_{C,i}(\xi_{C,i},\eta_{C,i},\zeta_{C,i}) - \mathbf{x}_T(\xi_T,\eta_T,\zeta_T)) = \mathbf{0} \tag{11}$$

with the Newton's method for the respective knot coordinates. By solving Eq. (11) for the knot coordinates ξ_T and η_T, the target point $\mathbf{x}_T$ closest to the current collocation point $\mathbf{x}_{C,i}$ is found. The distance g_n between the contact and target point is determined by

$$g_n = \mathbf{n}^T(\mathbf{x}_{C,i}(\xi_{C,i},\eta_{C,i},\zeta_{C,i}) - \mathbf{x}_T(\xi_T,\eta_T,\zeta_T)), \tag{12}$$

where the normal vector $\mathbf{n}$ is orthogonal to the surface of the target body. A positive normal gap g_n indicates a non-active contact. If the normal gap g_n is negative, the contact forces $\mathbf{f}_{C,i}$ and $\mathbf{f}_{T,i}$ of the contact and target body for the current collocation point are determined by

$$\mathbf{f}_{C,i} = +c_p g_n \mathbf{N}_C^T \mathbf{n} \hat{w}_i \qquad \text{and} \qquad \mathbf{f}_{T,i} = -c_p g_n \mathbf{N}_T^T \mathbf{n} \hat{w}_i, \tag{13}$$

where c_p is the penalty factor, $\mathbf{N}_C$ and $\mathbf{N}_T$ are the local shape functions, and $\hat{w}_i$ is the collocation weight of the current collocation point. See [9] for the derivation of the collocation weight. To eliminate the distinction between contact and target body, the roles are switched and the resulting contact forces are averaged. The resulting contact forces at each collocation point are assembled to the corresponding degree of freedom. The assembled vector ${}^I\mathbf{f}_{i,j,k}$ represents the contact force at each individual control point in the inertial frame K_I. Including the contact forces in the equations of motion (1) requires the determination of the discrete forces $\mathbf{h}_d$. The contact forces are transformed to the body frame by

$${}^R\mathbf{f}_{i,j,k} = \mathbf{S}_{IR}^T {}^I\mathbf{f}_{i,j,k}. \tag{14}$$

According to [1], the discrete forces $\mathbf{h}_d$ are computed with

$$\mathbf{h}_d = \sum_{i=1}^{n}\sum_{j=1}^{m}\sum_{k=1}^{\ell} \begin{bmatrix} {}^R\mathbf{f}_{i,j,k} \\ {}^R\mathbf{P}_{i,j,k} \times {}^R\mathbf{f}_{i,j,k} \\ \mathbf{\Phi}_{i,j,k}^T {}^R\mathbf{f}_{i,j,k} \end{bmatrix}. \tag{15}$$

Regarding the implementation, the contact search can be parallelized with respect to the collocation points $\mathbf{x}_{C,i}(\xi_{C,i},\eta_{C,i},\zeta_{C,i})$.

4.2 Quasistatic contact model

The concept of the quasistatic contact model is the partitioning of the equations of motion into "low" frequency (lf) modes and "high" frequency (hf) modes. The partitioning can be applied to

Eq. (1) resulting in

$$\begin{bmatrix} m\mathbf{E} & m\tilde{\mathbf{c}}^\mathsf{T} & \mathbf{C}_\mathrm{t}^{\mathrm{lf}\mathsf{T}} & \mathbf{C}_\mathrm{t}^{\mathrm{hf}\mathsf{T}} \\ m\tilde{\mathbf{c}} & \mathbf{I} & \mathbf{C}_\mathrm{r}^{\mathrm{lf}\mathsf{T}} & \mathbf{C}_\mathrm{r}^{\mathrm{hf}\mathsf{T}} \\ \mathbf{C}_\mathrm{t}^{\mathrm{lf}} & \mathbf{C}_\mathrm{r}^{\mathrm{lf}} & \overline{\mathbf{M}}_\mathrm{e}^{\mathrm{lf}} & \mathbf{0} \\ \mathbf{C}_\mathrm{t}^{\mathrm{hf}} & \mathbf{C}_\mathrm{r}^{\mathrm{hf}} & \mathbf{0} & \overline{\mathbf{M}}_\mathrm{e}^{\mathrm{hf}} \end{bmatrix} \begin{bmatrix} {}^\mathrm{R}\dot{\mathbf{v}}_\mathrm{IR} \\ {}^\mathrm{R}\dot{\boldsymbol{\omega}}_\mathrm{IR} \\ \ddot{\mathbf{q}}_\mathrm{e}^{\mathrm{lf}} \\ \ddot{\mathbf{q}}_\mathrm{e}^{\mathrm{hf}} \end{bmatrix} = \begin{bmatrix} \mathbf{h}_\mathrm{dt} \\ \mathbf{h}_\mathrm{dr} \\ \mathbf{h}_\mathrm{d}^{\mathrm{lf}} \\ \mathbf{h}_\mathrm{d}^{\mathrm{hf}} \end{bmatrix} + \begin{bmatrix} \mathbf{h}_\mathrm{bt} \\ \mathbf{h}_\mathrm{br} \\ \mathbf{h}_\mathrm{be}^{\mathrm{lf}} \\ \mathbf{h}_\mathrm{be}^{\mathrm{hf}} \end{bmatrix} - \begin{bmatrix} \mathbf{h}_{\omega\mathrm{t}} \\ \mathbf{h}_{\omega\mathrm{r}} \\ \mathbf{h}_{\omega\mathrm{e}}^{\mathrm{lf}} \\ \mathbf{h}_{\omega\mathrm{e}}^{\mathrm{hf}} \end{bmatrix} - \begin{bmatrix} \mathbf{0} \\ \mathbf{0} \\ \overline{\mathbf{K}}_\mathrm{e}^{\mathrm{lf}} \mathbf{q}_\mathrm{e}^{\mathrm{lf}} \\ \overline{\mathbf{K}}_\mathrm{e}^{\mathrm{hf}} \mathbf{q}_\mathrm{e}^{\mathrm{hf}} \end{bmatrix}, \tag{16}$$

where damping is neglected. It is shown in [5] that the "high" frequency modes only have small influence on the dynamical behavior and can be neglected in Eq. (16). Assuming quasistatic behavior of these modes leads to the following differential-algebraic system of equations of motion for a single body in contact

$$\begin{bmatrix} m\mathbf{E} & m\tilde{\mathbf{c}}^\mathsf{T} & \mathbf{C}_\mathrm{t}^{\mathrm{lf}\mathsf{T}} & \mathbf{0} \\ m\tilde{\mathbf{c}} & \mathbf{I} & \mathbf{C}_\mathrm{r}^{\mathrm{lf}\mathsf{T}} & \mathbf{0} \\ \mathbf{C}_\mathrm{t}^{\mathrm{lf}} & \mathbf{C}_\mathrm{r}^{\mathrm{lf}} & \overline{\mathbf{M}}_\mathrm{e}^{\mathrm{lf}} & \mathbf{0} \\ \mathbf{0} & \mathbf{0} & \mathbf{0} & \mathbf{0} \end{bmatrix} \begin{bmatrix} {}^\mathrm{R}\dot{\mathbf{v}}_\mathrm{IR} \\ {}^\mathrm{R}\dot{\boldsymbol{\omega}}_\mathrm{IR} \\ \ddot{\mathbf{q}}_\mathrm{e}^{\mathrm{lf}} \\ \mathbf{0} \end{bmatrix} = \begin{bmatrix} \mathbf{h}_\mathrm{dt} \\ \mathbf{h}_\mathrm{dr} \\ \mathbf{h}_\mathrm{d}^{\mathrm{lf}} \\ \mathbf{h}_\mathrm{d}^{\mathrm{hf}} \end{bmatrix} + \begin{bmatrix} \mathbf{h}_\mathrm{bt} \\ \mathbf{h}_\mathrm{br} \\ \mathbf{h}_\mathrm{be}^{\mathrm{lf}} \\ \mathbf{0} \end{bmatrix} - \begin{bmatrix} \mathbf{h}_{\omega\mathrm{t}} \\ \mathbf{h}_{\omega\mathrm{r}} \\ \mathbf{h}_{\omega\mathrm{e}}^{\mathrm{lf}} \\ \mathbf{0} \end{bmatrix} - \begin{bmatrix} \mathbf{0} \\ \mathbf{0} \\ \overline{\mathbf{K}}_\mathrm{e}^{\mathrm{lf}} \mathbf{q}_\mathrm{e}^{\mathrm{lf}} \\ \overline{\mathbf{K}}_\mathrm{e}^{\mathrm{hf}} \mathbf{q}_\mathrm{e}^{\mathrm{hf}} \end{bmatrix}. \tag{17}$$

The algebraic equations in the last row represent the balance of the contact forces $\mathbf{h}_\mathrm{d}^{\mathrm{hf}}$ and the inner forces $\overline{\mathbf{K}}_\mathrm{e}^{\mathrm{hf}} \mathbf{q}_\mathrm{e}^{\mathrm{hf}}$. These equations are essential to precisely represent the elastic deformations in the contact area. The differential-algebraic system (17) can be solved directly or the algebraic quasistatic contact equations are solved separately. Since the direct solution appears to be numerically challenging, the latter option is chosen. Therefore, the quasistatic contact equations

$$\mathbf{f}_\mathrm{qs}(\mathbf{q}_\mathrm{e}^{\mathrm{hf}}) = \mathbf{q}_\mathrm{e}^{\mathrm{hf}} - \left(\overline{\mathbf{K}}_\mathrm{e}^{\mathrm{hf}}\right)^{-1} \mathbf{h}_\mathrm{d}^{\mathrm{hf}}(\mathbf{r}_\mathrm{IR}, \boldsymbol{\beta}_\mathrm{IR}, \mathbf{q}_\mathrm{e}^{\mathrm{lf}}, \mathbf{q}_\mathrm{e}^{\mathrm{hf}}) = \mathbf{0} \tag{18}$$

need to be solved in every time step for the "high" frequency elastic coordinates $\mathbf{q}_\mathrm{e}^{\mathrm{hf}}$. This is achieved by Newton's method requiring the Jacobian $\mathbf{J}_\mathrm{qs}(\mathbf{q}_\mathrm{e}^{\mathrm{hf}})$ of Eq. (18). It is determined numerically by first order finite differences. To counter rounding and approximation errors of the Jacobian, a method to adjust the step size is applied [11]. Computing the Jacobian numerically in each Newton's iteration is highly expensive, due to the high number of elastic coordinates. To reduce computational effort, the Jacobian can be updated with Broyden's method [12]. In practice, the quasistatic contact model might become numerically challenging. This is the case when the penalty factor is too high and causes rank issues in Newton's method [3]. Therefore, the penalty factor needs to be chosen with care.

The developed quasistatic contact algorithm is detailed in Algorithm 1. The inputs of the quasistatic contact algorithm include the results of the previous time step. Among them are the "high" frequency elastic coordinates $\mathbf{q}_\mathrm{e}^{\mathrm{hf}}$, the Jacobian $\mathbf{J}_\mathrm{qs}(\mathbf{q}_\mathrm{e}^{\mathrm{hf}})$ of Eq. (18) and the Jacobian counter k_jac. Initially in line 1, Eq. (18) is checked for contact. If no contact occurs, the discrete forces $\mathbf{h}_\mathrm{d}^{\mathrm{lf}}$ are set to $\mathbf{0}$ in line 24. If a contact is detected, a while loop is initialized in line 4 to solve Eq. (18) with Newton's method. If the Jacobian counter k_jac is equal to its maximum $k_\mathrm{jac}^\mathrm{max}$ in line 5, a new Jacobian is determined in line 6 by numerically expensive first order approximation, and the Jacobian counter k_jac is reset. Otherwise, the previously with Broyden's method updated Jacobian is reused in line 9. Then, Newton's method is applied in line 11, and the counter k of the Newton iterations is increased in line 12. After the Newton step, the quasistatic equation (18) is evaluated in line 13 which is required for Broyden's method in line 14. Newton's method terminates successfully in line 15 and 18, if the solution does not change within the tolerance ε or the maximum number of Newton steps k^max is reached. Exceeding the maximum number of Newton steps k^max is non-critical, since in practice the stop criterion in line 15 is only minimally violated.

After the while loop, the discrete forces $\mathbf{h}_\mathrm{d}^{\mathrm{lf}}$ are determined in line 21 with Eq. (15), and the Jacobian counter k_jac is set back to 0. Therefore, the Jacobian can be used more than the $k_\mathrm{jac}^\mathrm{max}$ times. A wide range of numerical examples showed that this reduces the number of computed Jacobians while the results of the contact forces are nearly identical. Finally, the parameters $k_\mathrm{jac}^\mathrm{max} = 15$, $k_\mathrm{max} = 3 * k_\mathrm{jac}^\mathrm{max} = 45$, and $\varepsilon = 10^{-15}$ show efficient and robust behavior in tests.

Algorithm 1 Solution of the quasistatic contact equation (18).

Input: $\mathbf{q}_\mathrm{e}^\mathrm{hf}$, $\mathbf{J}_\mathrm{qs}(\mathbf{q}_\mathrm{e}^\mathrm{hf})$, k_jac

$\mathbf{f}_\mathrm{qs}(\mathbf{q}_\mathrm{e}^\mathrm{hf})$ {contact check Eq. (18)}
if contact **then**
  $k \leftarrow 0$ {Newton counter}
  while true **do**
    if $k_\mathrm{jac} = k_\mathrm{jac}^\mathrm{max}$ **then**
      $\mathbf{J}_\mathrm{qs}(\mathbf{q}_\mathrm{e}^\mathrm{hf})$ {new Jacobian}
      $k_\mathrm{jac} \leftarrow 1$ {reset counter}
    else
      $k_\mathrm{jac}{+}{+}$ {reuse Jacobian}
    end if
    $\mathbf{q}_{\mathrm{e},k+1}^\mathrm{hf} \leftarrow \mathbf{q}_{\mathrm{e},k}^\mathrm{hf} - \mathbf{J}_\mathrm{qs}(\mathbf{q}_\mathrm{e}^\mathrm{hf})^{-1}\mathbf{f}_\mathrm{qs}(\mathbf{q}_\mathrm{e}^\mathrm{hf})$
    $k{+}{+}$ {Newton counter}
    $\mathbf{f}_\mathrm{qs}(\mathbf{q}_\mathrm{e}^\mathrm{hf})$ {Eq. (18)}
    apply Broyden's method to $\mathbf{J}(\mathbf{q}_\mathrm{e}^\mathrm{hf})$
    if $\max(|\mathbf{q}_{\mathrm{e},k+1}^\mathrm{hf} - \mathbf{q}_{\mathrm{e},k}^\mathrm{hf}|) < \varepsilon$ **then**
      break {successful}
    else if $k = k^\mathrm{max}$ **then**
      break {successful}
    end if
  end while
  $\mathbf{h}_\mathrm{d}^\mathrm{lf}$ {discrete forces}
  $k_\mathrm{jac} \leftarrow 0$ {reuse Jacobian}
else
  $\mathbf{h}_\mathrm{d}^\mathrm{lf} \leftarrow \mathbf{0}$
  $k_\mathrm{jac} \leftarrow k_\mathrm{jac}^\mathrm{max}$ {new Jacobian}
end if

Output: $\mathbf{q}_\mathrm{e}^\mathrm{hf}$, $\mathbf{J}_\mathrm{qs}(\mathbf{q}_\mathrm{e}^\mathrm{hf})$, k_jac, $\mathbf{h}_\mathrm{d}^\mathrm{lf}$

4.3 Contact simulation procedure

This section introduces a contact simulation procedure including a contact detection, which allows switching the integration algorithm as well as its settings. Independent of a quasistatic contact, dividing a contact simulation into multiple phases, which are solved with different integration methods and settings, can be computational efficient. In the pre-impact phase, the elastic coordinates are not yet excited allowing larger step sizes. The impact phase requires the smallest step sizes due to high dynamics. In the post-impact phase the elastic coordinates are excited due to the impact but slightly larger step sizes are feasible compared to the impact phase. Additionally, the contact algorithm does not need to be evaluated until a new contact is detected. However, a contact search is needed to switch the simulation phase. In this work, the minimization of the distance function

$$f_\mathrm{d}(\xi_\mathrm{C}, \eta_\mathrm{C}, \zeta_\mathrm{C}, \xi_\mathrm{T}, \eta_\mathrm{T}, \zeta_\mathrm{T}) = \|\mathbf{x}_\mathrm{C}(\xi_\mathrm{C}, \eta_\mathrm{C}, \zeta_\mathrm{C}) - \mathbf{x}_\mathrm{T}(\xi_\mathrm{T}, \eta_\mathrm{T}, \zeta_\mathrm{T})\| \tag{19}$$

returns the points $\mathbf{x}_\mathrm{C}$ and $\mathbf{x}_\mathrm{T}$ on the contact and target body at which the two bodies are the closest. Here the MATLAB optimizer *fmincon()* is used. Another well known and computational more efficient approach is the use of bounding spheres [13]. However, the position of the closest points in the parameter space is in the scope of interest of future works. To reduce the computational effort of minimizing Eq. (19), the minimization is only performed every $\Delta t_\mathrm{search} = 100\,\mu\mathrm{s}$. As a consequence, the contact and target bodies can already penetrate each other in a pre- or post-impact phase. Since there must be no contact at the beginning of the impact phase, the over-calculated time steps are discarded until no more contact occurs. Then the impact phase begins.

The resulting procedure is visualized in Fig. 3. In the different phases, different integration methods and maximum step sizes have shown to be most efficient in numerical studies. The selection is additionally dependent on whether a contact according to Eq. (16) with modal damping or quasistatic contact is computed. The recommend settings are listed in Tab. 1. The maximum step size in the contact phase is determined by Nyquist–Shannon sampling theorem [14], where f^max is the maximum eigenfrequency within the flexible multibody system. The quasistatic contact simulation uses an explicit integrator. If an implicit integrator, e.g. MATLAB *ode15s()* or *ode23tb()*, is chosen, the solution of two nonlinear systems of equations will be chained into each other. Instead, *ode45()* is used with two modifications. First, contact forces and "high" frequency elastic coordinates are saved during the time integration. Otherwise, post-processing is as time-consuming as the simulation itself. Second, MATLAB integrators use variable step sizes. If an integration step is discarded, the initial conditions of Algorithm 1, i.e. the Jacobian $\mathbf{J}_\mathrm{qs}(\mathbf{q}_\mathrm{e}^\mathrm{hf})$, from the last successful step are used.

Essential functions, e.g. the contact evaluation in Section 4.1, the quasistatic contact in Section 4.2,

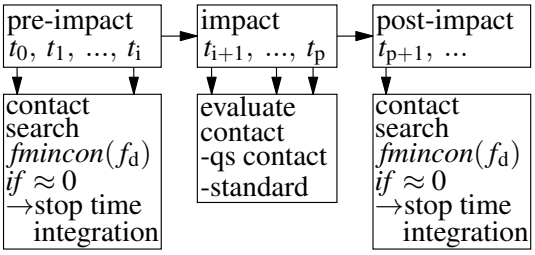

Figure 3: Procedure of the time simulation.

Table 1: Recommended integrator settings.

	modal damping	quasistatic
pre-impact	*ode15s()* $\Delta t_{\text{pre}}^{\max} = 100\,\mu\text{s}$	*ode23tb()* $\Delta t_{\text{pre}}^{\max} = 100\,\mu\text{s}$
impact	*ode15s()* $\Delta t_{\text{con}}^{\max} = \frac{1}{2f^{\max}}$	mod. *ode45()* $\Delta t_{\text{con}}^{\max} = \frac{1}{2f^{\max}}$
post-impact	*ode15s()* $\Delta t_{\text{post}}^{\max} = 100\,\text{ns}$	*ode23tb()* $\Delta t_{\text{post}}^{\max} = 100\,\mu\text{s}$

and the minimization of Eq. (19) are compiled into a MATLAB EXECUTABLE (MEX) files and parallelized if applicable.

5 APPLICATION EXAMPLE: IMPACT OF TWO FLEXIBLE DOUBLE PENDULUMS

This application example demonstrates the usage of a quasistatic contact model in a flexible multibody system with large rigid body motions. For comparison, a model reduced with Craig-Bampton method and modally damped "high" frequency modes is used. Due to the reduced numerical stiffness of the quasistatic contact model, it is expected that the quasistatic contact model will have lower computation times. Since the dynamics of the "high" frequency modes of the quasistatic contact model are neglected, the influence on accuracy is of interest. The setup is visualized in Fig. 4 and consists of two flexible double pendulums composed of elastic spheres and elastic connection rods. The locally refined IGA spheres are reduced with $n_{\text{q}}^{\text{lf}} = 25$ normal modes and $n_{\text{q}}^{\text{hf}} = 3 \times 218 = 654$ constraint modes. The rods are modeled by globally refined IGA models, which are modally reduced with $n_{\text{q}} = 20$ elastic coordinates. The double pendulum on the left-hand side in Fig. 4 is initially deflected by $\alpha_0 = 20^\circ$ and $\beta_0 = 21.14^\circ$. The two angles are chosen such that at the time of impact $\alpha = \beta = 0^\circ$ holds. Both pendulums are at rest at the beginning of the time simulation. The initial values of the elastic coordinates of the four flexible bodies need to be determined, since gravity is under consideration with $g = 9.81\,\text{m/s}^2$. A straightforward approach is to solve the equations of motion for the elastic coordinates $\mathbf{q}_{\text{e}}$ at the time $t = 0\,\text{s}$ such that the accelerations $\ddot{\mathbf{q}}_{\text{e}}$ vanish. Subsequently, the flexible multibody system is simulated for 200 ms. Due to initial deflection of the angles α_0 and β_0, the pre-impact phase consists of a large rigid body motion until the left pendulum impacts on the right pendulum. In the impact phase, the contact is evaluated and the elastic modes are excited. Finally, the post-impact phase includes a large rigid body motion. As a reference, a rigid body simulation with Hertzian contact [15] is chosen.
As mentioned before, the penalty factor c_{p} is determined heuristically by increasing it until the

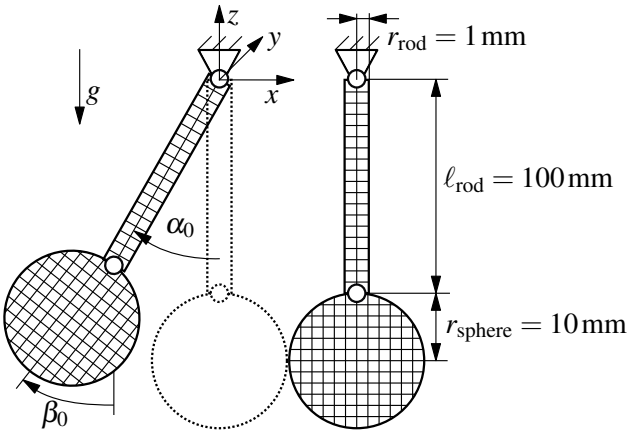

Figure 4: Simulation setup of two flexible double pendulums.

contact force converges. The procedure is visualized in Fig. 5. The maximum contact force is displayed in Fig. 5a and the required computation time in Fig. 5b. For the quasistatic contact model, the maximum possible penalty factor is $c_\mathrm{p} = 1 \times 10^{18}\,\mathrm{N/m}$. A further increase results in a singular Jacobian $\mathbf{J}_\mathrm{qs}$ of Eq. (18). Overall, the results of the maximum contact force in Fig. 5a show similar behavior between the two contact models. Significant differences are visible in Fig. 5b with respect to the computation time. The quasistatic contact model requires a fourth of the time of the modal damping model. With modal damping, the simulation needs approximately two hours for penalty factors less or equal than $c_\mathrm{p} = 1 \times 10^{18}\,\mathrm{N/m}$. The next higher value $c_\mathrm{p} = 2 \times 10^{18}\,\mathrm{N/m}$ requires almost twice the computation time. As mentioned before, increasing the penalty factor beyond its converging value also increases the numerical stiffness of the equations of motion, and, therefore, the computation time. An increase of the penalty factor beyond $c_\mathrm{p} = 1 \times 10^{18}\,\mathrm{N/m}$ only results in minor changes in the contact force, see Fig. 5a. Therefore, the penalty factor $c_\mathrm{p} = 1 \times 10^{18}\,\mathrm{N/m}$ is chosen.

The computation times for all three phases are listed in Tab. 2. The quasistatic contact model is faster in all three phases, especially in the post-impact phase. The major reduction of the computation time here can be explained with the reduced numerical stiffness of the quasistatic contact model. After the impact, only the "low" frequency modes are excited allowing larger step sizes.

Finally, the accuracy of the quasistatic contact model is investigated. The contact forces are visualized in Fig. 6. The overall time course in Fig. 6a and the visualization of the impact phase in Fig. 6b show good agreement between the quasistatic contact model and the modal damping model with the analytic solution by Hertz [15]. While the computation time of the quasistatic contact model is significantly reduced, the results are very similar to the modal damping model.

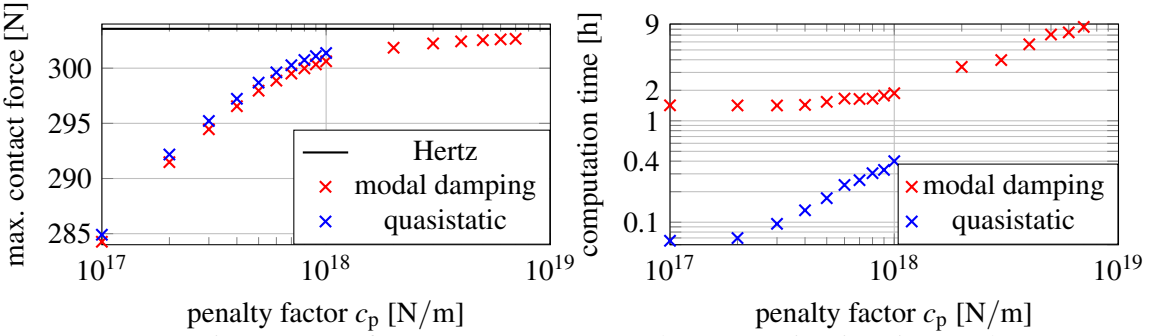

(a) Maximum contact force.

(b) Computation time (impact phase).

Figure 5: Convergence of the penalty factor.

Table 2: Computation times of the two double pendulums.

model	c_p	**pre-impact**	**impact**	**post-impact**
modal damping model	$1 \times 10^{18}\,\mathrm{N/m}$	9.5 min	1.9 h	15 h
quasistatic contact model	$1 \times 10^{18}\,\mathrm{N/m}$	16 s	24 min	1.3 min

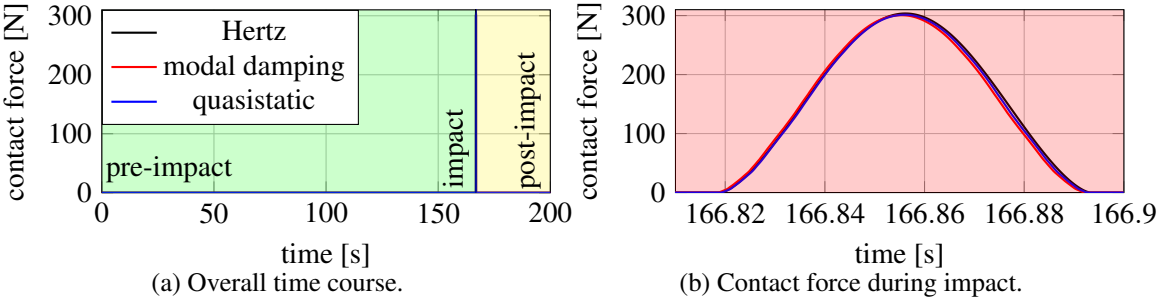

(a) Overall time course.

(b) Contact force during impact.

Figure 6: Time course of the contact force.

6 CONCLUSIONS

Overall, it can be concluded that a quasistatic contact model can be smoothly included in the floating frame of reference formulation. Subsequently, an impact simulation can be performed using the penalty formulation. The penalty factor converges for quasistatic contact models, and the differences in the accuracy between the quasistatic contact model and the modal damping model are minor. Due to the reduced numerical stiffness of the quasistatic contact model, the computational performance significantly improves compared to a modally damped contact model. The biggest difference occurs in the post-impact phase. Since the quasistatic contact equations (18) are numerically challenging to solve, the penalty factor could not be increased beyond its converging value in the application example. In a future work, this characteristic can be used to adaptively determine the penalty factor.

REFERENCES

[1] Schwertassek, R., Wallrapp, O.: Dynamik flexibler Mehrkörpersysteme (in German). Teubner B.G. GmbH (2014)

[2] Cottrell, J.A., Hughes, T.J.R., Bazilevs, Y.: Isogeometric Analysis. John Wiley & Sons, Ltd (aug 2009)

[3] Tschigg, S.: Effiziente Kontaktberechnung in Fexiblen Mehrkörpersystemen (in German). PhD thesis, Hamburg University of Technology (2020)

[4] Craig, R.R., Bampton, M.C.C.: Coupling of substructures for dynamic analyses. AIAA Journal **6**(7) (jul 1968) 1313–1319

[5] Tschigg, S., Seifried, R.: Efficient impact analysis using reduced flexible multibody systems and contact submodels. In: 6th European Conference on Computational Mechanics: Solids, Structures and Coupled Problems, ECCM 2018 and 7th European Conference on Computational Fluid Dynamics, ECFD 2018. (2018) 2711–2722

[6] Rückwald, T., Held, A., Seifried, R.: Hierarchical refinement in isogeometric analysis for flexible multibody impact simulations. Multibody System Dynamics (nov 2022)

[7] Les Piegl, W.T.: The NURBS Book. Springer-Verlag GmbH (1997)

[8] Bathe, K.J.: Finite Element Procedures. Klaus-Jürgen Bathe, United States Watertown, MA (2014)

[9] Matzen, M., Bischoff, M.: A weighted point-based formulation for isogeometric contact. Computer Methods in Applied Mechanics and Engineering **308** (aug 2016) 73–95

[10] Seifried, R., Hu, B., Eberhard, P.: Numerical and experimental investigation of radial impacts on a half-circular plate. Multibody System Dynamics **9**(3) (2003) 265–281

[11] Salane, D.E.: Adaptive routines for forming jacobians numerically. Sandia National Laboratories (1986)

[12] Broyden, C.G.: A class of methods for solving nonlinear simultaneous equations. Mathematics of Computation **19**(92) (1965) 577–593

[13] Wriggers, P.: Computational Contact Mechanics. Springer-Verlag GmbH (2006)

[14] Pintelon, R., Schoukens, J.: System Identification. John Wiley & Sons, Inc. (mar 2012)

[15] Johnson, K.L.: Contact Mechanics. Cambridge University Press (2004)